

NEUTRON DIFFRACTION POTENTIALITIES FOR NON-DESTRUCTIVE TESTING OF STRUCTURAL MATERIALS

V.V. Sumin¹, G.D. Bokuchava¹, I.V. Papushkin¹, A.M. Balagurov¹, A.M. Venter²

¹ *Joint Institute for Nuclear Research, Frank Laboratory of Neutron Physics, Dubna, Russia*

² *South African Nuclear Energy Corporation (NECSA), Pretoria, South Africa*

1. Introduction

Investigations of internal stresses using high resolution neutron diffraction were introduced about 20 years ago and became widespread due to many advantages in comparison with traditional techniques: high penetration depth, high spatial resolution, separate determination of strain anisotropy and stress distribution for each phase in multiphase materials, possibility to investigate magnetic as well as non-magnetic materials, possibility to investigate irradiative materials and components [1]. The proceedings of the last European and International conferences on residual stresses (ECSR-7 and ICSR-7) include a lot of reports on neutron scattering application for non-destructive testing.

Till now the Frank Laboratory of Neutron Physics, JINR, Dubna, is the only scientific centre in Russia where neutron diffraction is regularly used for internal stress studies and practical measurements. This work is conducted using correlation Fourier technique [2] on the high-flux IBR-2 reactor, which is a long-pulse type source with a pulse longer than 300 μ s for thermal neutrons. Since 1995, the high resolution Fourier diffractometer HRFD [3, 4] has been put in to routine operation at the IBR-2, and recently, the second Fourier machine (FSD) intended for stress experiments was constructed [5, 6]. In this paper, the current situation with FSD is reported and several examples of performed experiments are given.

2. FSD design and performance

The FSD design satisfies the requirements of high luminosity, high resolution, specific sample environment, wide range of d_{hkl} , and fixed scattering angles $\pm 90^\circ$. It consists of mirror neutron guide, fast Fourier chopper for the neutron beam intensity modulation, VME-based RTOF-analyzers for data acquisition and wide aperture detector system. A distinguishing feature of the detector system is that it includes two multielement ZnS(Ag)/⁶LiF scintillator-based detectors at scattering angles $\pm 90^\circ$ with combined electronic and geometric focusing [7]. Being flexible, the scintillation screen allows each element of the detector to approximate the time focusing surface of the scattered neutrons with required accuracy. At the same time, the modern electronics provides the addition of signals from separate detector elements on a single time-of-flight scale. This combination leads to a sharp increase of the solid angle of the detector system and, as a result, to an increase of its luminosity, preserving a high interplanar spacing resolution, i.e., on the level $\Delta d/d \approx 4 \cdot 10^{-3}$. A minimum measured gauge volume is $2 \times 2 \times 2$ mm³. A typical measuring time for single diffraction spectrum is 2÷4 hours.

The resolution function of FSD was estimated from high-resolution neutron diffraction spectra measured on α -Fe standard sample (Fig. 1) by three detectors (one backscattering and two 90° detectors) at maximal Fourier chopper speed $V_{max}=6000$ rpm. Results of experiments shown that all detectors have sufficiently high-resolution and wide enough range of d_{hkl} : $\Delta d/d \approx 2 \cdot 10^{-3}$ for backscattering detector and $\Delta d/d \approx 4 \cdot 10^{-3}$ for 90° detectors at $d_{hkl} = 2$ Å (Fig. 2). It was shown that final electronically focused spectra possess the same level of resolution as measured with the individual detector module.

The sample environment includes the following equipment which is used during experiments: 5-axis goniometer for total strain tensor measurements, two load testing machines (up to 20 kN and 60 kN), mirror furnace for material studies at temperatures up to 2000°C.

In the frame of the joint JINR – NECSA project “Neutron Scattering Applications” the new mechanical loading machine LM-20 for tensile/compressive tests with force and temperature control was purchased and adopted on FSD diffractometer. Furthermore the multisectional radial collimator system for -90° detector was produced and installed.

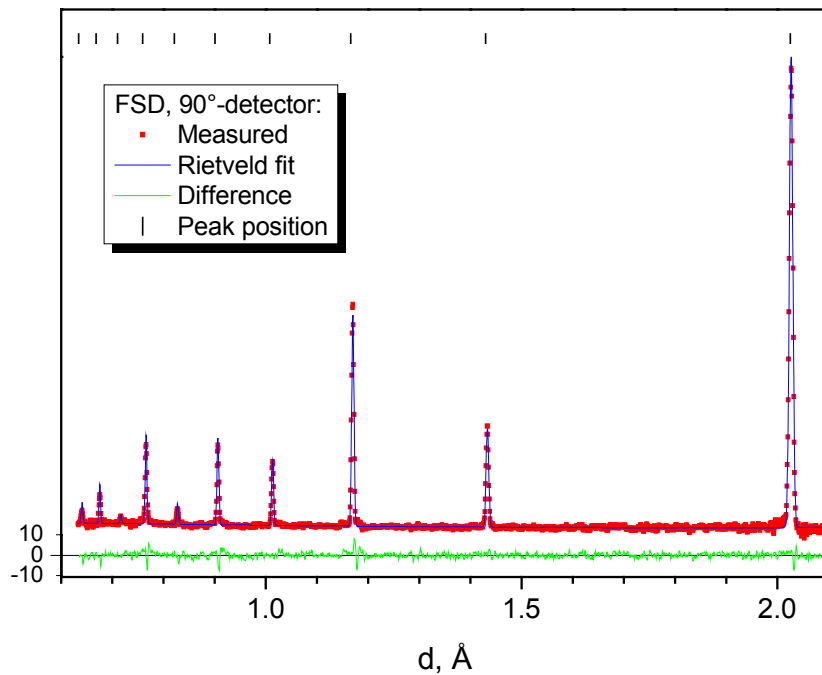


Fig. 1. Part of neutron diffraction pattern from the α -Fe standard sample measured by 90° detector. Experimental points, profile calculated by the Rietveld method and difference curve are shown.

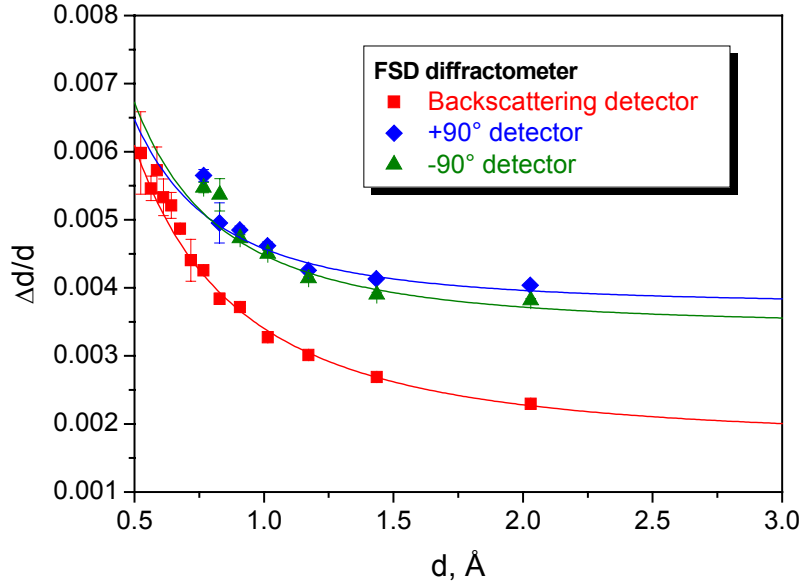


Fig. 2. FSD resolution function measured on α -Fe standard sample at maximal Fourier chopper speed $V_{max} = 6000$ rpm.

3. Radial collimator system

Multisectional radial collimator of FSD diffractometer is designed for gauge volume definition within the bulk of the studied sample during strain scanning (Fig. 3). The radial collimator consists of 4 independent modules (two 7° and two 10° acceptance angle modules). Each module is made of mylar films coated with gadolinium oxide (total thickness about $50 \mu\text{m}$). Individual module of the radial collimator can be mechanically adjusted to optimize the geometry of the experiment (Fig. 4).

All four radial collimator modules has been constructed and manufactured in PNPI (Gatchina, Russia). Performed test experiments have shown that the radial collimator provides 2 mm space resolution and improves significantly the gauge volume definition within the bulk of the sample (Fig. 5). At present residual stress scanning in the depth of the material using radial collimator became a routine procedure on FSD. In Fig. 6 the relationship between the gauge volume coordinate and diffraction peak intensity is shown. When the gauge volume is only partially filled by the material a slow increase in peak intensity is observed (Region 1). The intensity maximum is reached then the gauge volume is totally filled by the material (Region 2). At the same time at deeper gauge volume position peak intensity exhibits exponential decrease due to neutron attenuation effect (Region 3). In this case diffraction peak intensity dependence is well described by the following formula: $I = I_0 \exp(-\mu D)$, where μ is attenuation coefficient of the material, D is total path of the neutron beam within material. Therefore precise sample surface position determination is possible with accuracy of 0.1 mm (or even better) by the help of radial collimator.

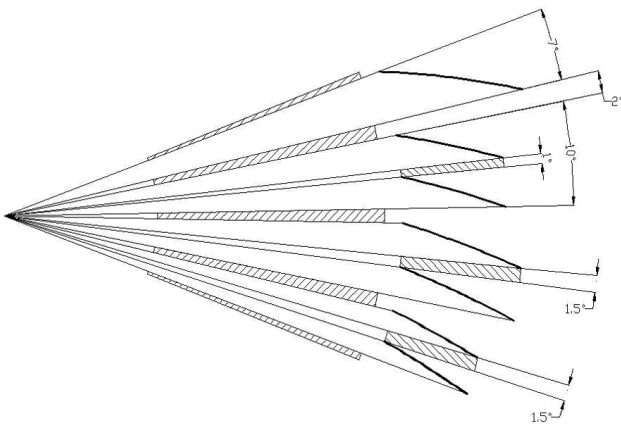


Fig. 3. Multisectonal radial collimator arrangement with respect to flexible $\text{ZnS(Ag)}^6\text{LiF}$ scintillation screens of 90° detector. Shaded areas are collimator's and detector's walls, correspondingly.

Fig. 4. Multisectonal radial collimator system with spatial resolution of 2 mm: currently 7° and 10° modules of radial collimator are installed on FSD.

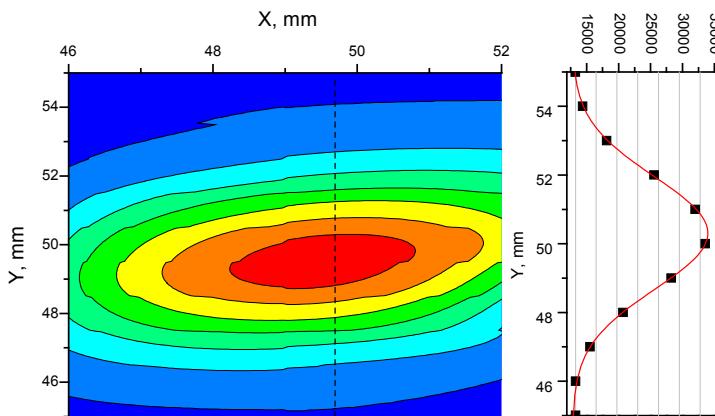


Fig. 5. Gauge volume definition: neutron intensity distribution map for radial collimator. Incident beam width was 10 mm. Measured spatial resolution function for radial collimator ≈ 2 mm.

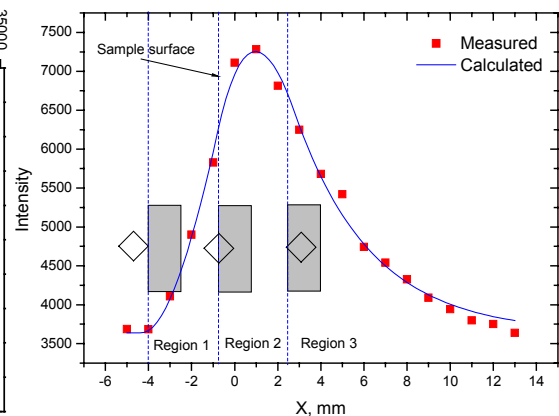


Fig. 6. Sample surface scan using radial collimator: diffraction peak intensity versus gauge volume position in the bulk of material.

4. New mechanical testing machine LM-20

As a part of the sample environment modernization the new uniaxial mechanical testing machine LM-20 was purchased in Nuclear Physics Institute of the Czech Academy of Sciences (Řež near Prague). This mechanical testing machine provides tensile and compressive load on the sample with maximal value up to 20 kN. Main advantage of this construction is almost play-free load transfer to a sample (Fig. 7). Additionally there is a possibility to heat investigated sample up to 800 °C (with temperature control by Eurotherm controller). LM-20 electronics can be easily integrated with FSD diffractometer control system in order to provide on-line experiments execution. Normally M12 screw threaded cylindrical samples are used in LM-20 for tensile/compressive tests. Sample length can vary within 30÷100 mm range (Fig. 8).

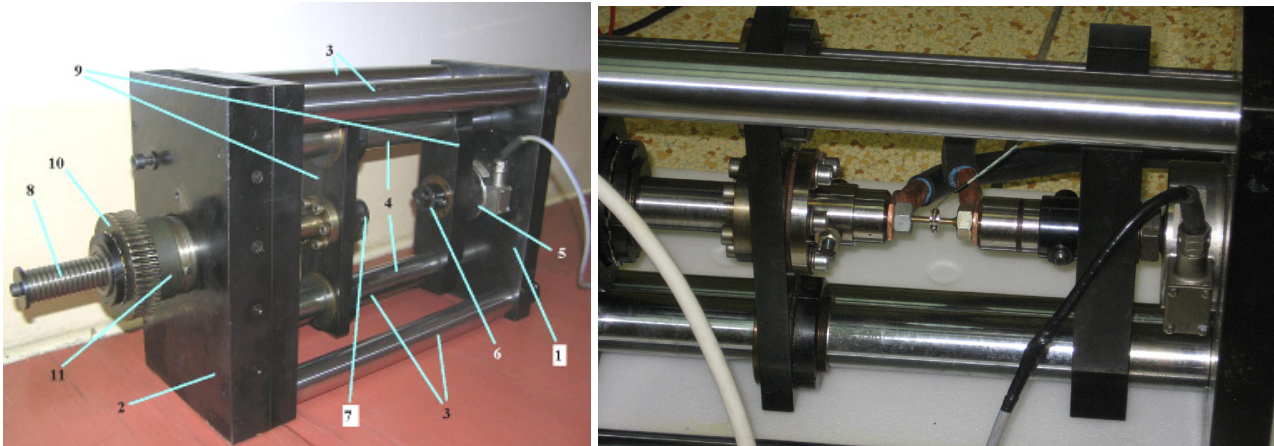


Fig. 7. Left: uniaxial mechanical testing machine LM-20: stationary part of the machine is metallic frame consisting of two parallel platforms /1/ and /2/. These platforms are connected with six cylindrical rods. Four of these rods /3/ are basic load-bearing elements of construction and two others /4/ serves for rigid fixation of the load axis. In the centre of the bottom platform /1/ force measuring device /5/ is mounted. /6/ and /7/ are upper and bottom part of the sample grips is connected to device /5/. The upper part of the sample grip /7/ is rigidly fixed with load axis of the machine via platform /9/ using bolted connections. Load is transferred to sample by step motor using gear /10/ and screw /11/ mechanism. Right: LM-20 testing machine with investigated steel sample heated by direct current.



Fig. 8. From left to right: a) typical samples; b) investigated steel sample with mechanical extensometer; c) sample heating by direct current.

Main advantages of LM-20 testing machine are sufficient load range, possibility to operate in horizontal and vertical position, operation at elevated temperatures, compact size, reliability,

flexible software, reasonable price. Working parameters of the LM-20 testing machine are the following: maximal load - ± 20 kN, temperature range - up to 800 °C, sample dimensions - 30÷100 mm, sample elongation control – by mechanical extensometer, device control – by PC (Windows/VME).

During test experiments in FLNP JINR steel sample installed in LM-20 machine was subjected to multiple tensile and compressive load cycles with various rates and amplitudes of the applied force. Additionally several tests were conducted with sample heating by electric current up to 500 °C. Temperature stability during these tests was about 0.1 °C. Since ReMeSys control software allows one to run any combination of applied force and temperature on the sample several cycling tests were performed using these two parameters. In whole it should be mentioned that examination of LM-20 mechanical testing machine was successful: the device corresponds to the claimed parameters and it is stable in use. Since the LM-20 machine is fully automatic device and is supplied with equipment for temperature regulation the new wide possibilities for investigation of mechanical properties of various materials and units are now opened.

5. Calibration of FSD diffractometer

a) In order to characterize FSD sensitivity to spatial strain determination the four-point bend experiment was performed. Al alloy sample was subjected to in situ deformation in four-point bending device, and at the same time spatial strain distribution in the bulk of the material was studied using neutron diffraction (Fig. 9). According to the elasticity theory four-point bended sample deformation has a linear dependence from pure tension at down part to pure compression at upper one (without shear deformation).

Experimental values of lattice strain determined from diffraction peak shifts are shown in Fig. 10. It can be clearly seen that spatial strain distribution is well described by linear dependence as it was predicted by elasticity theory.

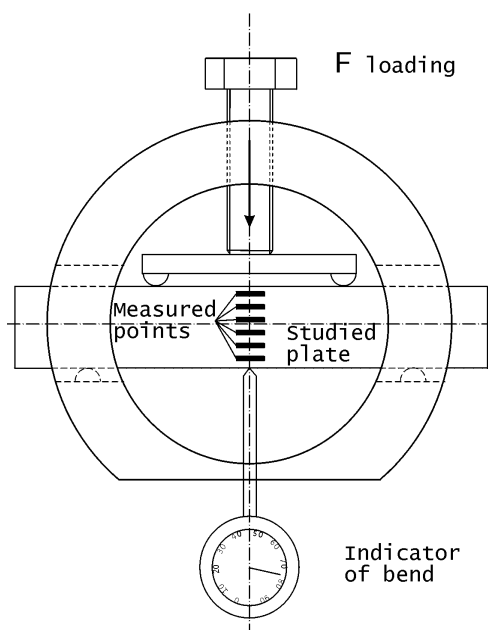


Fig. 9. Four point bending device with test sample. Scan points are shown in bold.

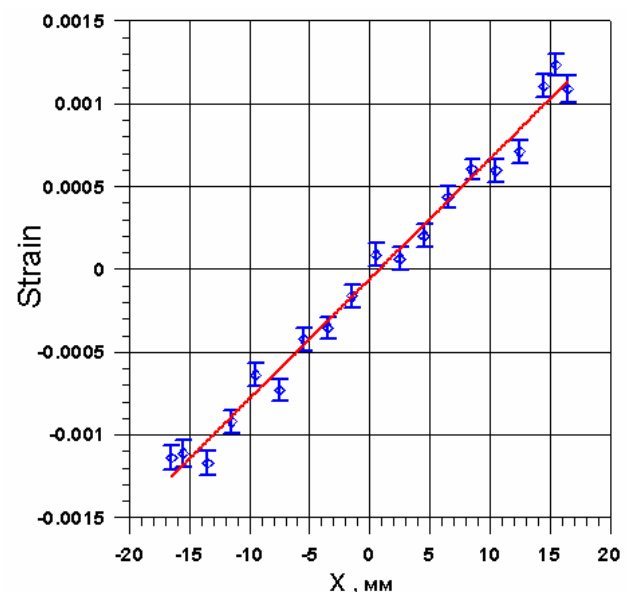


Fig. 10. Lattice strain spatial distribution versus X coordinate. $X = 0$ corresponds to the center of the plate.

b) In the frame of spectrometer calibration a set of experiments for Young's modulus determination for D16 Al alloy (Russian grading) was performed. Samples were subjected to uniaxial applied load in "TIRAtest 2560" stress rig in-situ in neutron beam. Applied load was measured by "DMS Kraftaufnehmer" dynamometer (first grade of accuracy device) while total macroscopic deformation was measured using "MiniMFA" mechanical extensometer installed on the sample. At

the same time by the help of neutron diffraction lattice strain was determined from relative lattice parameter change $\varepsilon = \Delta a/a$ at given value of applied stress σ ($\sigma = F/S$, where F is applied force, S is sample cross-section).

In Fig. 11 elastic lattice strain versus applied load is shown for all four studied samples. In good agreement to the elastic theory this dependencies are linear for applied load up to 370 MPa. At higher load values studied material undergoes plastic deformation (sample Nr.4) and, consequently, in this case lattice strain exhibits clearly seen deviation from linear dependence ($\varepsilon > 0.005$). From the slopes of the strain-stress linear dependencies Young's modules for investigated material were obtained. Mean value $\langle E \rangle = 68.62 \pm 0.82$ GPa for D16 Al alloy fits well to reference value given in literature $E = 70.3$ GPa [8]. Minor difference between experimental and reference values can be explained by slight variation in chemical composition and thermal treatment of the samples.

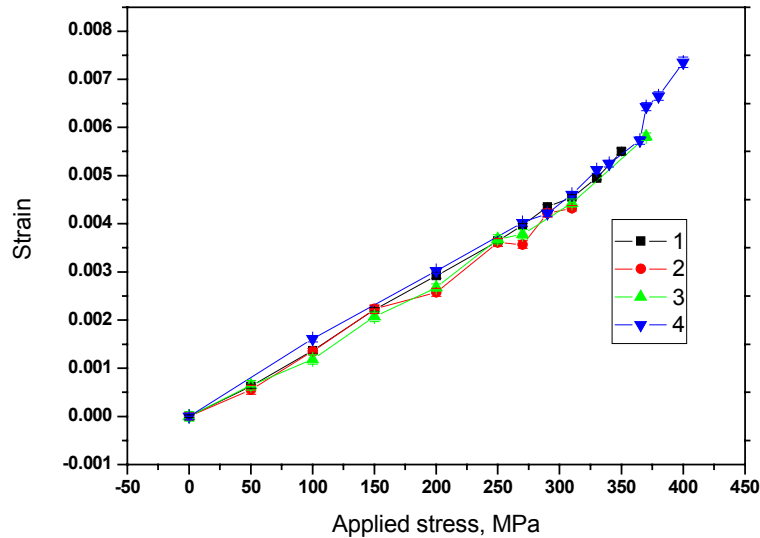


Fig. 11. Elastic lattice strain versus applied load. Sample Nr. 4 undergoes plastic deformation.

6. Standardization of Neutron Technique

In the framework of the Project “NET - European Network on Neutron Techniques Standardization for Structural Integrity” round robin sample TG1 with single weld bead on plate (Fig. 12) was investigated on FSD diffractometer [9]. Task Group 1 (TG1) has the main objective to standardize residual stress measurement techniques on the benchmark, yet industrially valuable, case of a single weld bead-on-plate problem and as such contributes to the overall NeT Network objective. On the other hand, TG1 aims at the equally important objective of validating the finite element method for simulating welding and predicting residual stresses, by comparing predicted with measured data in the benchmark case of a single weld bead-on-plate. All performed measurements were consistent with the recommendations stated in ISO/TTA 3:2001: Determination of Residual Stresses by Neutron Diffraction. The details of input measurements, welding, residual neutron measurements, and finite element calculations can be found in [9].

Residual strains were measured on FSD diffractometer along weld bead starting from the $X = 0$ (center of the bead) to the $X = 80$ mm (sample edge) where stresses due to welding procedure are almost absent (Fig. 13). For these measurements the gauge volume of $3 \times 3 \times 3$ mm³ dimensions was defined by the boron nitride mask. Time-of-flight neutron diffraction method allowed to measure 8 reflections simultaneously. All reflections were fitted by Rietveld methods to estimate lattice parameter at each point. Measurements made away from the weld at $X = 80$ mm, was used as the stress free reference value of lattice parameter. The results of the measurements of residual stress distribution in TG1 round robin sample were in good agreement with results received at ISIS (UK), NPI (Prague, Czech Republic), JRC (Petten, Netherlands) and Helmholtz Zentrum Berlin.

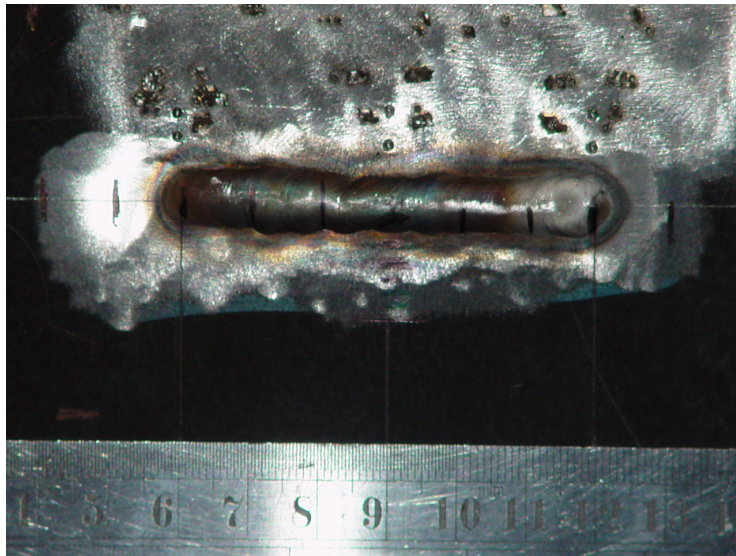


Fig. 12. Single weld bead-on-plate specimens (round robin sample TG1) on stainless steel plate $120 \times 180 \times 17 \text{ mm}^3$, for details see [9].

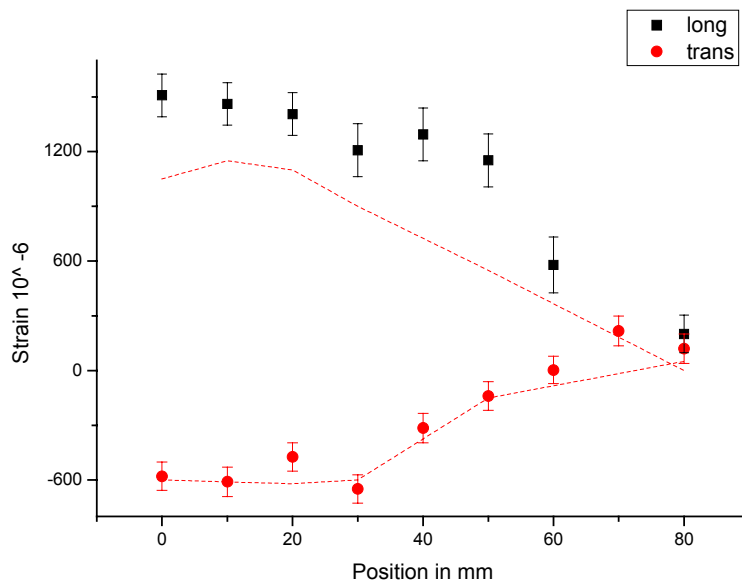


Fig. 13. Longitudinal (■) and transversal (●) strain component measured at FSD at depth 3 mm along the weld bead starting from the center of the weld. Data obtained in JRC (Petten) are represented by dashed lines.

7. Example of FSD applications

A number of experiments, characterizing main directions in this research field were performed on HRFD and FSD. As concerns to reactor material science the following samples were studied: bimetallic joints [10], austenitic build-up welding on ferritic steel, weld seams. Furthermore, mechanical properties of austenitic steel at various load conditions (including cyclic load) were investigated [11]. Residual stresses, phase contents and mechanical properties in new perspective materials – gradient structures and composites – were studied [12]. The results of these neutron experiments are already used for materials technology and machinery optimization.

Within the framework of co-operation with Ministry of Atomic Energy of Russia the test experiments on residual stress study in welded VVER-1000 reactor vessel were carried out. The method of welding of an austenite steel layer on a ferrite steel reactor core is frequently used to increase corrosion resistance and strength of such component. The residual stress investigations in such two-layer components are important for the development of optimal techniques for applying

strengthening layers. The sample was made of two steel layers: the main layer with thickness of 34 mm - ferrite steel 15XГМΦАА (in Russian notation) and the welded layer with thickness of 9 mm - austenite steel 12X18H10T (in Russian notation). The residual stresses measured by neutron diffraction and two mechanical (crack propagation and cutting) methods are shown in Fig. 14. It is necessary to note that significant compressive σ_y stress component under build-up welding decreases crack corrosion probability under operating load. The partial discrepancy between obtained results can be explained by the methodological differences of applied experimental techniques.

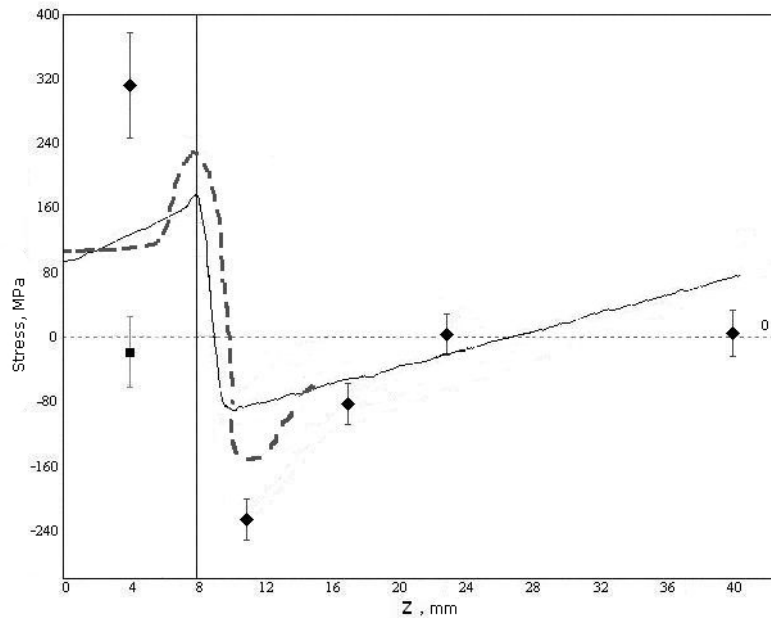


Fig. 14. Residual stresses in studied template along phase interface. Vertical line indicates austenite-ferrite interface position at $Z = 8$ mm. Points represent residual stresses measured by neutron diffraction parallel to phase interface (♦ - σ_y , ■ - $\sigma_x \approx \sigma_z$). Dash curve represents stress kinetic intensity value obtained using crack propagation method while solid curve corresponds to the residual stress value estimated by cutting method.

Another example of FSD application is investigation of mechanical properties of austenitic steel under applied uniaxial load by neutron diffraction method. Austenitic stainless steels are widely used in engineering because of their high corrosion resistance and toughness. Therefore it is necessary to control mechanical properties of a material at various load regimes. Elastic properties depend on the state of material, chemical composition, microstructure and mechanical and thermal treatment. Therefore it is necessary to determine experimentally the elastic constants for the studied material. The examined material was the austenitic stainless steel X6CrNiTi1810 of the following content (wt. %): C - 0.04, Si - 0.44, Mn - 1.14, P - 0.033, S - 0.004, Cr - 17.74, Ni - 19.3, Ti - 0.35. The sample of the austenitic steel was subjected to the applied load in situ in the neutron beam, using a special purpose loading device. The elastic strain was measured for different crystal planes (hkl) with scattering vector \vec{Q} direction parallel and perpendicular to the applied load (Fig. 15). Strain in parallel direction was measured at the scattering angle $2\theta = 90^\circ$, in perpendicular direction - at the scattering angle $2\theta = 152^\circ$. Moreover, average strain was determined independently by extensometers from relative changes of sample dimensions. For all registered spectra separate diffraction peak positions and widths were determined. Strains for all available crystal planes (hkl) were obtained from relative shift of diffraction peaks. Also diffraction spectra were processed by Rietveld profile refinement method. In this case strain averaged on all crystallographic directions [hkl] and corresponding to the anisotropy factor $\Gamma_{hkl} = 0.2$ were obtained from lattice parameter changes. In plastic region (at the applied stress level over ~ 250 MPa) strain registered by extensometers deviates from linear dependence. On the contrary strain obtained from neutron

diffraction data does not show strong deviation from linear dependence. At that a width of diffraction peak increases significantly (Fig. 16). Such behavior of diffraction peak is typical for plastic deformation regime. In elastic region the elastic modules $E_{hkl}^{||}$ and E_{hkl}^{\perp} as a function of the anisotropy factor $\Gamma_{hkl} = (h^2k^2 + h^2l^2 + k^2l^2)^2 / (h^2 + k^2 + l^2)^2$ were obtained from the slopes of the strain-stress linear dependencies. The elastic constants S_{11} , S_{12} and S_{44} were calculated in the frame of the Hill model [13] which assumes taking of an arithmetic average of the Reuss and Voigt model values and gives the results very close to the Kröner model values. Thus, the following values were obtained for the investigated austenitic stainless steel: $S_{11} = 6.70 \cdot 10^{-6} \text{ MPa}^{-1}$, $S_{12} = -2.24 \cdot 10^{-6} \text{ MPa}^{-1}$, and $S_{44} = 12.43 \cdot 10^{-6} \text{ MPa}^{-1}$.

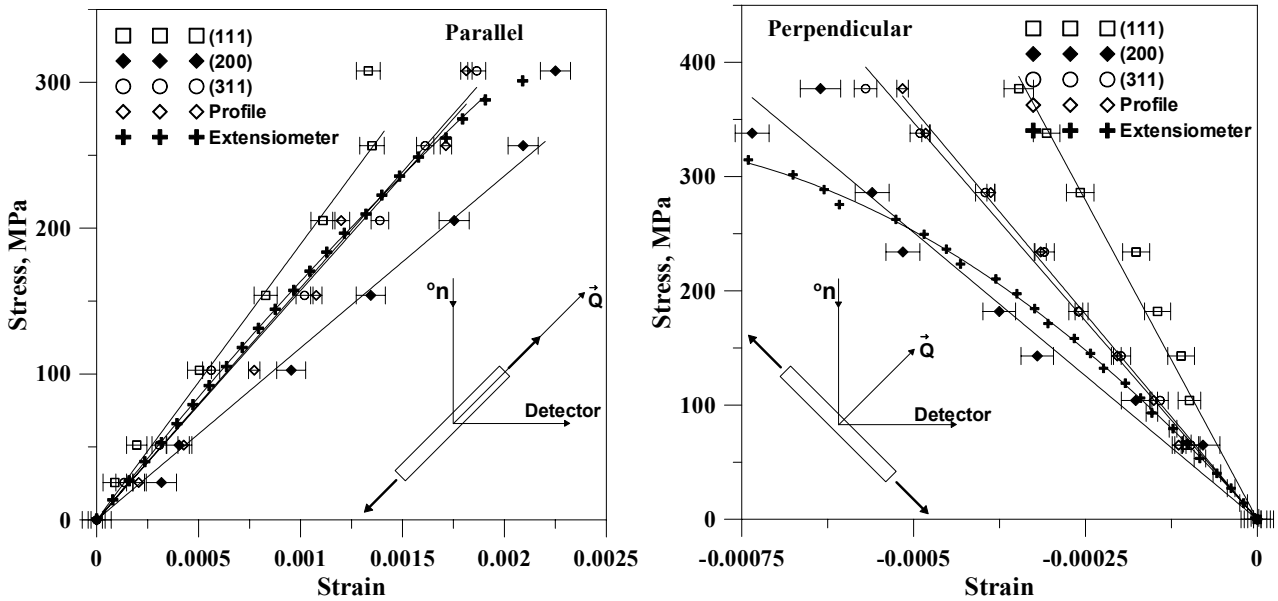


Fig. 15. Lattice strain parallel (left) and perpendicular (right) to applied load.

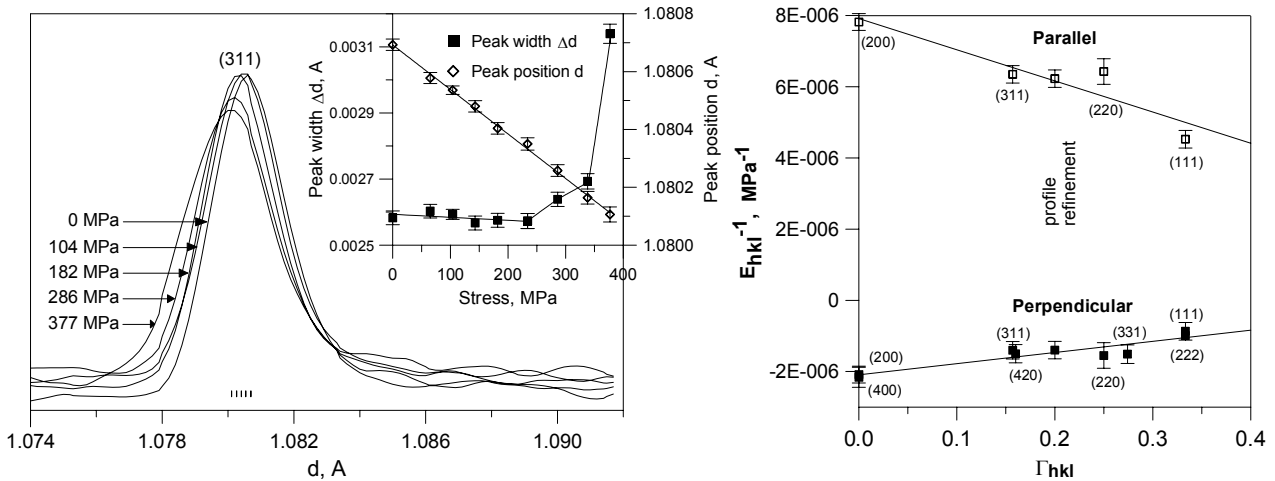


Fig. 16. Bragg reflection (311) position and width changes versus applied load (left). Dependence of the elastic modules $E_{hkl}^{||}$ and E_{hkl}^{\perp} parallel and perpendicular to the applied load versus the anisotropy factor Γ_{hkl} (right).

8. Conclusions

The performed experiments have shown that the FSD parameters confirm the fitness of the diffractometer for residual stress studies with required accuracy of 20 - 30 MPa. High resolution of diffractometer ($\Delta d/d \approx 4 \cdot 10^{-3}$) allows one to characterize mechanical properties of the materials at room and elevated temperatures with good precision. At the same time spatial strain distribution study in bulk industrial samples became a routine procedure using radial collimator system.

Acknowledgement

The authors wish to acknowledge the help of many members of the FLNP JINR (Dubna) and PNPI of RAS (Gatchina) staff in engineering, fabrication and installation of the FSD instrument. This work was supported in the frame of the joint JINR – NECSA project “Neutron Scattering Applications” and by IAEA under research contract No. 13737 “Application of Reverse Time of Flight (RTOF) Neutron Diffraction for Residual Stress Investigations”.

REFERENCES

1. Measurements of residual stress in materials using neutrons. IAEA-TECDOC-1457, IAEA, 2005.
2. Hiismaki P., Poyry H., Tiitta A., J. Appl. Cryst. 1988. V. 21. P. 349.
3. Aksenov V.L., Balagurov A.M., Simkin V.G. et al., J. Neutron Research, 5 (1997) 181.
4. A.M. Balagurov, “High resolution Fourier diffraction at the IBR-2 reactor” Neutron News, 2005, v.16 (3), pp.8-12.
5. G.D. Bokuchava et al., “Neutron Fourier diffractometer FSD for internal stress analysis: first results”, Applied Physics A: Materials Science & Processing, v.74 [Suppl1] (2002) pp s86-s88.
6. Balagurov A.M., Bokuchava G.D., Kuzmin E.S. et al., “Neutron RTOF diffractometer FSD for residual stress investigation”, Zeitschrift für Kristallographie, Supplement Issue No. 23 (2006) 217-222.
7. E.S. Kuzmin, A.M. Balagurov, G.D. Bokuchava et al., “Detector for the FSD Fourier diffractometer based on ZnS (Ag)/6LiF scintillation screen and wavelength shifting fiber readout”, J. of Neutron Research, Vol. 10, Nr 1 (2002) 31-41.
8. I.C. Noyan, J.B. Cohen. Residual stress. Measurement by diffraction and interpretation. Springer-Verlag, 1987, 275 p.
9. C. Ohms, R.C. Wimpory, D.E. Katsareas, A.G. Youtsos, “NeT TG1: Residual stress assessment by neutron diffraction and finite element modelling on a single bead weld on a steel plate”, Intern. J. of pressure vessels and piping (2009) v. 86, Nr. 1, pp. 133-230.
10. A.V. Tamonov, V.V. Sumin, “Investigation of residual stresses in bimetallic stainless steel – zirconium adapter by neutron diffraction”, J. of Neutron Research, 12 (2004) 69.
11. G.D. Bokuchava, V.V. Luzin, J. Schreiber and Yu.V. Taran, “Residual stress investigations in austenitic steel samples with different degree of low cycle fatigue”, Textures and Microstructures, 33 (1999) 279-289.
12. G.D. Bokuchava, J. Schreiber, N. Shamsutdinov, M. Stalder, “Residual stress studies in graded W/Cu materials by neutron diffraction method”, Physica B: Condensed Matter 276-278 (2000) 884-885.
13. Hill, R. (1952). Proc. Phys. Soc. A65, 349-354.